






Review

# Catalytic Activity of Rare Earth Elements (REEs) in Advanced Oxidation Processes of Wastewater Pollutants: A Review

Lorenzo Saviano <sup>1,†</sup>, Antonios Apostolos Brouziotis <sup>1,2,†</sup> , Edith Guadalupe Padilla Suarez <sup>1</sup>, Antonietta Siciliano <sup>1,\*</sup> , Marisa Spampinato <sup>1,3</sup>, Marco Guida <sup>1,3</sup> , Marco Trifuoggi <sup>2,4</sup> , Donatella Del Bianco <sup>1</sup>, Maurizio Carotenuto <sup>5</sup>, Vincenzo Romano Spica <sup>6</sup> , Giusy Lofrano <sup>6</sup> and Giovanni Libralato <sup>1</sup>

<sup>1</sup> Department of Biology, University of Naples Federico II, 80126 Naples, Italy; lorenzo.saviano@unina.it (L.S.); antonis.brouziotis@outlook.it (A.A.B.); edithguadalupe.padillasuarez@unina.it (E.G.P.S.); marisa.spampinato@unina.it (M.S.); marguida@unina.it (M.G.); donatelladelbianco09@gmail.com (D.D.B.); giovanni.libralato@unina.it (G.L.)

<sup>2</sup> Department of Chemical Sciences, University of Naples Federico II, 80126 Naples, Italy; marco.trifuoggi@unina.it

<sup>3</sup> NBFC, National Biodiversity Future Center, 90133 Palermo, Italy

<sup>4</sup> CeSMA Advanced Metrological and Technological Service Center, University of Naples Federico II, 80126 Naples, Italy

<sup>5</sup> Department of Chemistry and Biology “Adolfo Zambelli”, University of Salerno, 84084 Fisciano, Italy; mcarotenuto@unisa.it

<sup>6</sup> Department of Movement, Human and Health Sciences, University of Rome “Foro Italico”, 00135 Rome, Italy; vincenzo.romanospica@uniroma4.it (V.R.S.); glofrano@unisa.it (G.L.)

\* Correspondence: antonietta.siciliano@unina.it; Tel.: +39-0812534641

† These authors contributed equally to this work.



**Citation:** Saviano, L.; Brouziotis, A.A.; Suarez, E.G.P.; Siciliano, A.; Spampinato, M.; Guida, M.; Trifuoggi, M.; Del Bianco, D.; Carotenuto, M.; Spica, V.R.; et al. Catalytic Activity of Rare Earth Elements (REEs) in Advanced Oxidation Processes of Wastewater Pollutants: A Review. *Molecules* **2023**, *28*, 6185. <https://doi.org/10.3390/molecules28176185>

Academic Editor: Xiaomin Xu

Received: 21 June 2023

Revised: 12 August 2023

Accepted: 18 August 2023

Published: 22 August 2023



**Copyright:** © 2023 by the authors. Licensee MDPI, Basel, Switzerland. This article is an open access article distributed under the terms and conditions of the Creative Commons Attribution (CC BY) license (<https://creativecommons.org/licenses/by/4.0/>).

**Abstract:** In recent years, sewage treatment plants did not effectively remove emerging water pollutants, leaving potential threats to human health and the environment. Advanced oxidation processes (AOPs) have emerged as a promising technology for the treatment of contaminated wastewater, and the addition of catalysts such as heavy metals has been shown to enhance their effectiveness. This review focuses on the use of rare earth elements (REEs) as catalysts in the AOP process for the degradation of organic pollutants. Cerium and La are the most studied REEs, and their mechanism of action is based on the oxygen vacancies and REE ion concentration in the catalysts. Metal oxide surfaces improve the decomposition of hydrogen peroxide to form hydroxide species, which degrade the organics. The review discusses the targets of AOPs, including pharmaceuticals, dyes, and other molecules such as alkaloids, herbicides, and phenols. The current state-of-the-art advances of REEs-based AOPs, including Fenton-like oxidation and photocatalytic oxidation, are also discussed, with an emphasis on their catalytic performance and mechanism. Additionally, factors affecting water chemistry, such as pH, temperature, dissolved oxygen, inorganic species, and natural organic matter, are analyzed. REEs have great potential for enhancing the removal of dangerous organics from aqueous solutions, and further research is needed to explore the photoFenton-like activity of REEs and their ideal implementation for wastewater treatment.

**Keywords:** rare earth elements; catalytic activity; advanced oxidation processes; aqueous solutions

## 1. Introduction

Over the past few decades, conventional wastewater treatment plants (WWTPs) showed low efficiencies in removing contaminants of emerging concern (CECs) [1–3]. CECs encompass a wide range of substances, including pharmaceuticals, personal care products, and dyes [1,4].

The chronic release of these substances in water bodies represents a serious threat to human health and ecosystems and requires urgent advancements in wastewater treatment technologies [5–7] focusing also on the perspective of treated wastewater reuse.

Advanced oxidation processes (AOPs) evidenced potential revolutionary solutions in the development of integrated systems for the treatment of contaminated wastewater [1,8]. The mechanism of action of AOPs relies on the generation of reactive oxygen species (ROS) with strong oxidation capabilities, such as hydroxyl ( $\text{OH}\cdot$ ), sulfate ( $\text{SO}_4^{2-\cdot}$ ), and superoxide ion radicals ( $\text{O}_2^{-\cdot}$ ), which quickly degrade a wide range of organic compounds in  $\text{CO}_2$ ,  $\text{H}_2\text{O}$ , and inorganic acids [9–11]. The addition of catalysts, such as heavy metals, can promote the development of such radicals and improve the process efficiency [12–14].

AOPs, particularly Fenton oxidation, are commonly carried out under acidic conditions, leading to the consumption of significant amounts of acid and base reagents [15,16]. The effectiveness of AOPs relies on the proper dosage of reactive hydroxyl (HO) radicals, ensuring the desired level of treatment is achieved [17,18]. A major limitation of AOPs is their relatively high cost, primarily due to the use of expensive chemicals and increased energy consumption [17]. Additionally, AOPs can result in the formation of unknown recalcitrant by-products, which may be more nephrotoxic than the original compounds, posing unresolved challenges [1,7]. While AOPs are effective in scavenging reactive radicals from non-target substances, they may not be suitable for certain categories of toxic compounds that resist degradation by HO radicals.

Recently, the application of rare earth elements (REEs) in the advanced oxidation process (AOP) has gained growing interest [19]. The REEs are a group of seventeen chemical elements in the periodic table, the 15 lanthanides from lanthanum (La) to lutetium (Lu), to which scandium (Sc) and yttrium (Y) are added since the latter tend to occur in the same mineral deposits with lanthanides and exhibit similar chemical properties. REE ions have a particular electronic structure compared to transition metal ions and are gaining great importance as Lewis acids in Green Chemistry because they can be used in aqueous solvents or water without any deactivation; they can be easily recovered from the reaction medium by extraction and can be used several times without loss of activity [19,20]. The redox properties of REEs depend on the arrangement of the surfaces and the shape and size of their crystals, and, for this reason, they can be improved by checking the nanostructure [21].

REEs exhibit unique physicochemical properties, such as high surface area, reactivity, and redox potential [22]. These properties make REEs suitable to be used in AOPs, where they can enhance the performance of the processes [23,24]. REEs can be used as catalysts to promote the generation of reactive oxygen species (ROS) when exposed to UV radiation in photocatalysis processes [25], to catalyze Fenton-like processes [26], and to enhance the efficiency of ozonation by increasing the production of hydroxyl radicals [27].

To date, most applications are still at lab scale and an increasing number of studies are being performed to fill the existing gaps in the usage of REEs for polluted water treatment. The main limitations to full-scale applications deal with high energy and capital cost.

This review focuses on the use of REEs as catalysts for the degradation of CECs from wastewater, since their use, which is currently in place for wastewater treatment, lacks processing and economic sustainability.

## 2. Methodology of Data Collection

The REE-assisted catalytic removal of CECs has substantially grown in recent decades, as retrieved in a Scopus search (keywords: rare earth elements, catalyst, and wastewater) updated on 20 December 2022.

We have collected 60 papers dealing with the degradation of different CECs from wastewater using REEs in AOPs. As shown in Figure 1a where the number of papers issued each year on catalytic removal of contaminants in wastewater treatment using REEs have been reported, the first publication was made in 1995 [28], which means that the field is quite new. Since 2015, the number of publications has been increasing each year. Figure 1b shows the cumulative number of publications for each REE over the period of 1995–2022. Most processes were carried out by using Ce and La. Cerium has received by far most of

the attention (148 publications), followed by La (44), Y (10), and Nd (10). Five REEs (Sc, Ho, Tm, Lu, and Pm) and their possible effective role in this field have never been explored.

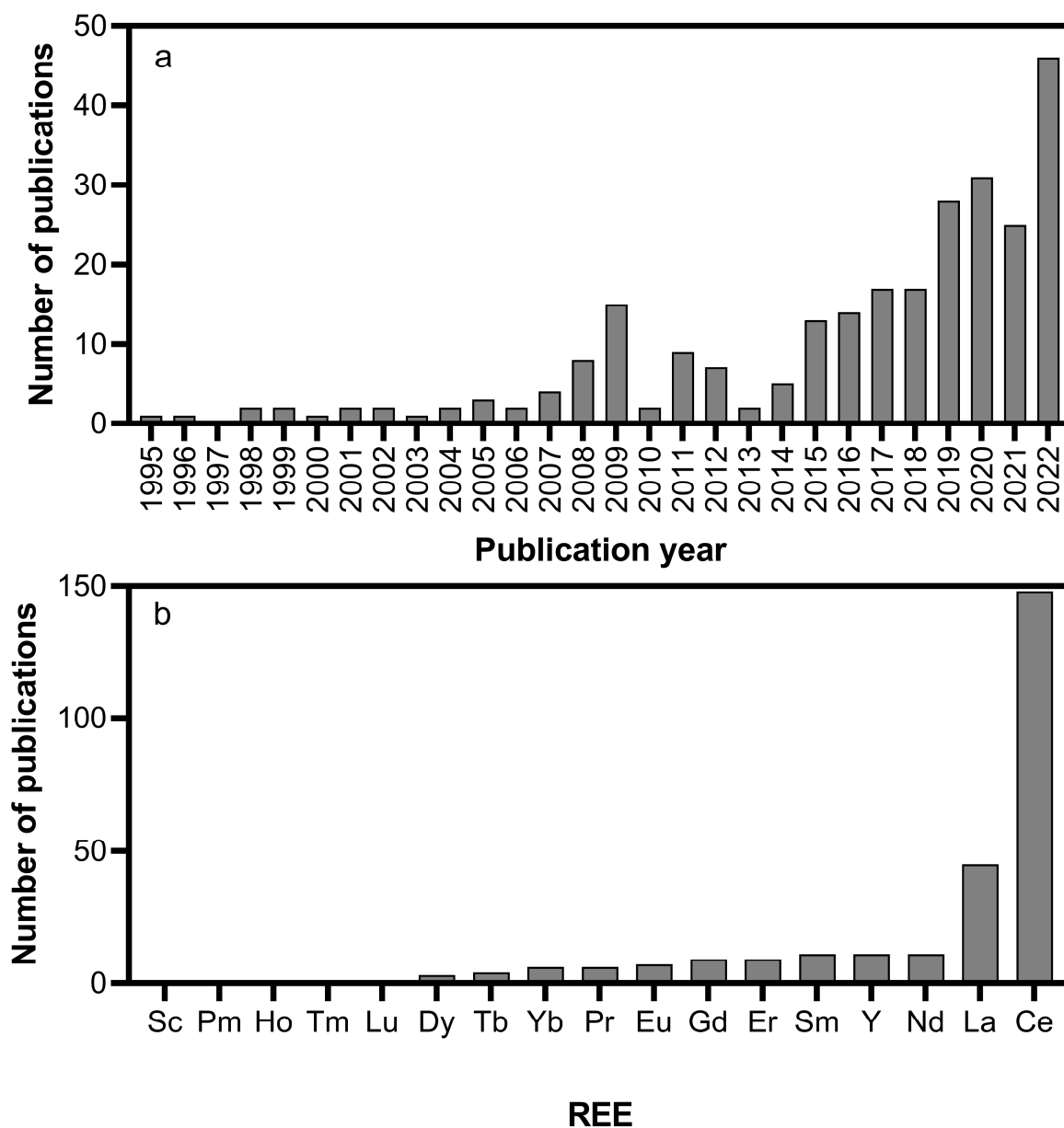


**Figure 1.** (a) The number of papers issued each year on catalytic removal of contaminants in wastewater treatment using REEs over the period of 1995–2022; (b) a cumulative number of publications for each REE over the period of 1995–2022.

Figure 2 presents the distribution of research papers that focused on the utilization of REE catalysts for the degradation of various types of contaminants. According to the data, pharmaceutical compounds and dyes accounted for the highest percentage of research papers, with approximately 33% and 42%, respectively. Alkaloids, herbicides, phenols, organic acids, cyanides, and other contaminants were also investigated to a lesser extent, each representing 3–8% of the papers. This distribution highlighted the varying levels of research emphasis on different categories of contaminants in relation to REE catalysts in the past.

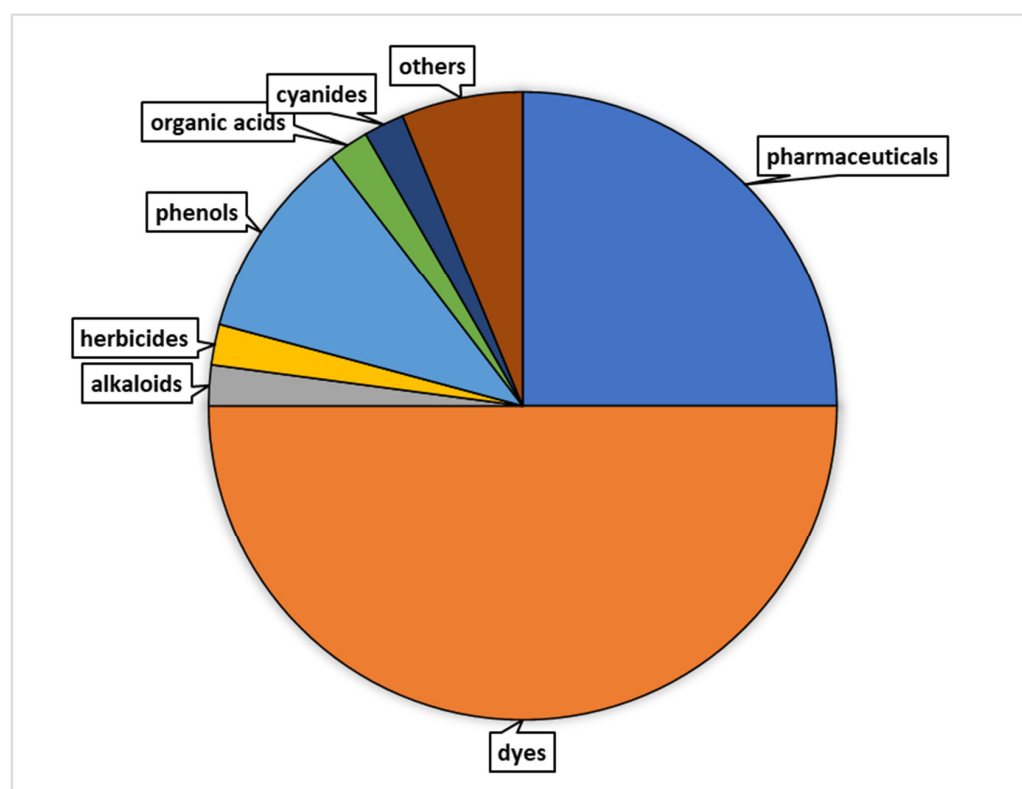


**Figure 2.** Percentage distribution of research papers on the utilization of REE catalysts for the degradation of different contaminant types.

The chemical, metallurgical, and physical properties of the REEs are governed by their electron configuration. In contrast to element Y, the lanthanides are characterized by the progressive filling of the 4f orbital [29]. Due to the low energy of these electrons, they do not directly participate in the bonding when forming compounds with other elements. As a consequence, this leads to a significant similarity in the chemical reactivity of the lanthanides. This uniform reactivity pattern is evident consistently throughout geochemical processes, rather than being unique to each individual element [29,30].

In Table 1, the essential details encompassing the atomic numbers and intricate valence shell electronic configurations pertaining to the distinctive set of REEs are provided.

**Table 1.** Atomic Number and Valence Shell Electronic Configuration of the Rare Earth Elements.

Element	Atomic Number	Valence Shell Electronic Configuration
Y	39	[Ar] 3d1 4s2
La	57	[Ar] 4d1 5s3
Ce	58	[Xe] 4f1 5d1 6s2
Pr	59	[Xe] 4f3 5d0 6s2
Nd	60	[Xe] 4f4 5d0 6s2
Pm	61	[Xe] 4f5 5d0 6s2
Sm	62	[Xe] 4f6 5d0 6s2
Eu	63	[Xe] 4f7 5d0 6s2
Gd	64	[Xe] 4f7 5d1 6s2
Tb	65	[Xe] 4f9 5d0 6s2

Table 1. Cont.

Element	Atomic Number	Valence Shell Electronic Configuration
Dy	66	[Xe] 4f10 5d0 6s2
Ho	67	[Xe] 4f11 5d0 6s2
Er	68	[Xe] 4f12 5d0 6s2
Tm	69	[Xe] 4f13 5d0 6s2
Yb	70	[Xe] 4f14 5d0 6s2
Lu	71	[Xe] 4f14 5d1 6s2

### 3. AOP-Based REEs for CECs Removal

#### 3.1. Pharmaceutical Degradation

Pharmaceutical toxic compounds can end up in wastewater via many routes, such as via their consumption by humans or their use in agriculture. Therefore, it is essential to discover effective ways for decomposing these hazardous compounds in wastewater. The use of REEs has been shown by several studies to be potentially useful. Numerous researchers utilized REEs in various forms as heterogeneous catalysts in AOPs (Table 1).

Nie et al. [31] carried out a Fenton-like reaction, at 30 °C, to take complete degradation of the antibiotic sulfamethoxazole (SMX), in the simultaneous presence of LaFeO<sub>3</sub> and H<sub>2</sub>O<sub>2</sub> at pH values ranging between 5.5 and 7.14. It was found that the SMX removal efficiency increased with the increase of the catalyst load and then reached a constant value when the LaFeO<sub>3</sub> concentration was above 1.4 g/L. Furthermore, it was investigated that the LaFeO<sub>3</sub> could be reused for at least 10 cycles and the reused catalyst kept the catalytic activity nearly as efficient as the fresh one. Ref. [32] investigated the photocatalytic activity for degradation of carbamazepine and caffeine using MIL-125-NH<sub>2</sub>, LaFeO<sub>3</sub>, and LaFeO<sub>3</sub>/MIL-125-NH<sub>2</sub> photocatalysts under solar simulator at ambient temperatures. LaFeO<sub>3</sub>/MIL-125-NH<sub>2</sub> composite exhibited higher carbamazepine and caffeine degradation than MIL-125-NH<sub>2</sub> MOF and LaFeO<sub>3</sub> perovskite and this is highlighted through the calculation of pseudo-first-order kinetics equation. LaFeO<sub>3</sub>/MIL-125-NH<sub>2</sub> composite photocatalysts prepared by the self-assembly method have shown excellent and promising results in the degradation of pharmaceutical compounds.

Chen et al. (2022) [33] used LaFeO<sub>3</sub>/lignin-biochar (LFO/LG) catalysts prepared by a sol-gel pyrolysis to evaluate the degradation of ofloxacin (OFX) under visible light irradiation. The pure LaFeO<sub>3</sub> (LFO) and the pure lignin-biochar (LG) were tested and prepared under the same conditions to compare which one had the best performance. The whole process was operated at a constant temperature in the presence of H<sub>2</sub>O<sub>2</sub> (30 wt%) and all experiments were carried out under different initial pH, revealing later an optimal photodegradation efficiency at pH values above 6. In addition, the morphology, microstructure, energy band structure, and photoelectrochemical behavior of the composite catalysts were characterized and the relationship with catalytic performance was explained. Pure LFO has almost no adsorption of OFX when the system was left in the dark to reach a saturation adsorption state and the degradation efficiency for LFO is only 53.4% after a 75-min degradation reaction. Instead, LFO-LG samples showed a significant adsorption effect on OFX, and the degradation efficiency was also improved up to 95.6%.

In the study of [34], the electrochemical degradation of dipyrone using cerium catalysts was not effective during a two-hour electrolysis. However, the use of a CeO<sub>2</sub>/C gas diffusion electrode degraded all of the dipyrone in 20 min with 26% mineralization at −1.3 V, and after only 5 min with 57% mineralization at −1.1 V when the Fenton process was employed. The authors declared that ceria acts as an oxygen buffer leading to an increase in the local oxygen concentration, facilitating H<sub>2</sub>O<sub>2</sub> formation and consequently improving the dipyrone degradation. FeCeO<sub>x</sub> can remove 83% of diclofenac in a heterogenous Fenton process and can be reused due to its chemical stability [35].

A heterogeneous Fenton catalyst, Ce<sup>0</sup>-Fe<sup>0</sup>-reduced graphene oxide (Ce-Fe-RGO), showed good catalytic performance and adsorption of sulfamethazine [13]. Ferrum-doped CeO<sub>2</sub> nanosheets with various Fe/Ce ratios were evaluated for the Fenton-like degradation of salicylic acid (SA). The 2% Fe-doped CeO<sub>2</sub> nanosheets showed the highest concentration of surface oxygen vacancies and catalytic activity under the optimum reaction conditions due to the complex adsorption of SA and H<sub>2</sub>O<sub>2</sub> on the surface Ce<sup>3+</sup>. The catalytic activity of the nanosheets could be recovered, and so they could be reused in new cycles [36]. A surface of graphite felt loaded with CeO<sub>x</sub> accelerated the mineralization of carbamazepine via an E-peroxone process [37].

The Fe<sup>0</sup>/CeO<sub>2</sub> nanocomposite enhanced the removal of tetracycline (TC) in the Fenton oxidation process and could be reused for further cycles. The authors suggested a synergistic effect between nanoscale Fe<sup>0</sup> and CeO<sub>2</sub> [19].

Hu et al. [38] tried out for the first time the use of cobalt (Co) and REE gadolinium (Gd) to investigate the removal of two antibiotics from wastewater, ciprofloxacin (CIP) and tetracycline. In particular, the sponge-like structure of Co- and Gd-modified biochar (MBC) was conducive to studying its adsorption capacity due to the presence of metal oxides and functional groups. Furthermore, the influence of pH on the absorption of antibiotics was studied by varying the pH between 3 and 11. It was observed that at pH 9, the antibiotic adsorption capacity of MBC was greatly increased. These data suggested that MBC is an innovative and effective adsorbent for the removal of antibiotics from complex contaminated water.

Luan et al. [39] synthesized photocatalysts Er<sub>2</sub>FeSbO<sub>7</sub>, BiTiSbO<sub>6</sub>, or N-TO by solid-state method to degrade enrofloxacin (ENR), a common antibiotic able to effectively kill Gram-positive and Gram-negative bacteria and mycoplasma under visible light irradiation. A new photocatalyst provided by Er<sub>2</sub>FeSbO<sub>7</sub>/BiTiSbO<sub>6</sub> heterojunction (EBH) was prepared for the first time by the thermal solvent method and tested. It was observed that the photocatalytic activity among the four photocatalysts was as follows: EBHP > Er<sub>2</sub>FeSbO<sub>7</sub> > BiTiSbO<sub>6</sub> > N-TO. Therefore, it can be concluded that the EBHP process can be a potent method for treating pharmaceutical wastewater that is polluted by ENR.

In general, the studies highlighted the use of diverse catalysts to improve the efficiency of removing pharmaceutical compounds. Each study focused on targeting specific pharmaceutical compounds; this targeted approach allowed for a more accurate evaluation of the catalyst's performance against particular contaminants. Among the studies conducted on CIP removal, the highest removal percentage (>99%) within a timeframe of 180 min was achieved by the study utilizing the MBC catalyst [38].

The pH can play a significant role in the reactivity and adsorption behavior of both the catalyst and the target compound. The studies reported a range of pH values, including pH 4, 5, 6.48, and 9, indicating that different pH levels can be effective depending on the specific catalyst and target compound.

Furthermore, the temperature of the reaction can influence the reaction kinetics and the stability of the catalyst. It was generally observed that moderate temperatures (20–25 °C) were preferred to strike a balance between reaction rates and energy consumption.

The pharmaceutical degradation studies highlighted the potential of Fenton-based processes for wastewater treatment, showcasing the reusability of FeCeO<sub>x</sub> [33], the catalytic performance and adsorption properties of Ce-Fe-RGO [13], and the degradation capabilities of ferrum-doped CeO<sub>2</sub> nanosheets [19]. The results emphasize the versatility and effectiveness of Fenton processes in removing pharmaceutical compounds, offering promising solutions for the treatment of wastewater contaminated with these contaminants.

### 3.2. Dye Degradation

Wastewater from the textile industry contains residual dyes which are hardly biodegradable. Advanced Oxidation Processes (AOPs) are alternative techniques for the destruction of dyes and many other organic products in wastewater and effluents. In Table 2, the degradation efficiency of various dyes using REE catalysts is highlighted, including the

type of contaminant, initial concentration, reaction conditions, and the corresponding degradation percentage achieved by the REE catalysts.

**Table 2.** REEs studied for simple photocatalysis and Fenton-like photocatalysis.

Type of Reaction	REEs Studied
Photocatalysis	Y, La, Ce, Nd, Sm, Eu, Gd, Tb, Dy, Er, Yb
Fenton-like catalysis	Y, La, Ce, Pr, Nd, Eu, Gd, Dy, Yb

The presence of La in the La–Fe montmorillonite (La–Fe MMT) composite enhanced the degradation efficiency of the organic dyes Rhodamine B (RhB) and methylene blue (MB) and resulted in a little iron leaching, consequently increasing the lifetime of the system. Due to its low cost, efficient reactivity, high stability, and low metal leaching, it seems a great potential as a green catalyst for the heterogeneous Fenton-like degradation of hazardous dyes [40]. FeOCl doped with Y or La showed efficient Fenton catalytic activity for ibuprofen degradation under simulated solar light [41]. Tungsten oxide composites (WO<sub>3</sub>) doped with La, Gd, or Er showed an enhanced photocatalytic degradation of organic dyes compared to the pure composites [42].

Huang et al. (2014) [43] doped hydroxyl FeAl intercalated montmorillonite with La or Ce and saw an improvement in the photo-Fenton catalytic oxidation of Reactive Blue 19 under natural sunlight irradiation. The photo-Fenton activity of pristine CoFe<sub>2</sub>O<sub>4</sub> on the oxidation of five organic dyes was enhanced by inserting a very small quantity of La or Ce cations into its spinel structure in the presence of two different oxidants [44].

Divya and Renuka (2015) [45] doped nanoceria with five different elements (Cu, Fe, Zr, Dy, and La) and investigated the heterogeneous Fenton-like oxidation of MB. CuO showed the highest catalytic activity, which is attributed to the synergistic effect between copper and ceria. The Cu–Mn/CeO<sub>2</sub>/SBA-15 catalysts can efficiently degrade (>99%) high-concentration dye pollutants. The excellent catalytic performance could be attributed to the well-dispersed catalytic nanoparticles inside the mesopores and the catalytic synergic effect of CeO<sub>2</sub> [46]. Xie, Yibing, and Chunwei Yuan [47] showed that Ce<sup>4+</sup>-TiO<sub>2</sub> sol and nanocrystallites can photodegrade the reactive brilliant red dye (X-3B) with the dye/Ce<sup>4+</sup>-TiO<sub>2</sub>/visible-light reaction system.

Singh et al. (2016) [48] prepared several Cu/zeolite Y catalysts to test the decolorization, degradation, and mineralization of recalcitrant diazo dye (Congo red) in a heterogeneous Fenton-like process. The catalyst with 7.5 wt% Cu showed the maximum degradation, decolorization, and mineralization of 93.58%, 95.34%, and 79.52% after 2.5, 2, and 4 h, respectively, along with reproducible activity for three cycles. The addition of Y on the surface of BiW<sub>2</sub>O<sub>6</sub> composites enhanced the degradation of RhB compared to the individual composites under visible light illumination, by producing holes (h<sup>+</sup>) and superoxide radicals [49].

Seroglazova et al. (2022) [50] showed that Praseodymium orthoferrite (PrFeO<sub>3</sub>) nanopowders can achieve 100% efficiency of photo-Fenton-like degradation of methyl violet. The PrFeO<sub>3</sub>/CeO<sub>2</sub>-based nanocomposites can degrade methyl violet (MV) under the presence of visible light via a photocatalytic Fenton-like activity. These nanoparticles can be reused due to their stability and be separated from the reaction solution [51]. In the study of [52], Pr–CdWO<sub>4</sub> nanoparticles could degrade the toxic synthetic azo dye Remazol Black B by 93.9% at optimal conditions.

Nd-doped ZnO nanoneedles can degrade MB under UV light. Especially 1% Nd can degrade 2.5 times more with respect to undoped ZnO [53]. The LaFeO<sub>3</sub> perovskites exhibit better photocatalytic activity towards the oxidative degradation of dye molecules when doped with Nd, Eu, Gd, or Dy [54].

Keerthana et al. (2021) [55] showed that zinc ferrite (ZnFe<sub>2</sub>O<sub>4</sub>) nanoparticles doped with 2% Samarium (Sm) can remove 65% of MB dye with the help of visible light irradiation within 1 h and, due to their stability, could be reused for more than three cycles. In the study

of [56], Sm-doped CeO<sub>2</sub> nanoparticles demonstrated a very efficient photodegradation of UV-irradiated rose bengal dye. Wang et al. (2017) [57] showed that Sm-doped Bi<sub>2</sub>MoO<sub>6</sub> photocatalysts could degrade more effectively RhB with respect to the individual particles.

The europium-nitrogen (EueN) co-doped TiO<sub>2</sub>/Sepiolite nanocomposites, prepared through microwave-hydrothermal treatment, can be used to effectively eliminate dyestuff in real wastewater treatment. In particular, in order to evaluate the degradation of an anionic dye, Orange G, the photocatalytic activities were conducted under solar irradiation. The Eu-N co-doped TiO<sub>2</sub>/Sep NCs, with various amounts of Eu<sup>III</sup>, photocatalysts exhibited improved photoactivity as compared to mono-doped and undoped samples [58]. In other studies, europium, in the +2 and +3 oxidation state, has been used as a dopant in VOC degradation over metal oxide catalysts such as TiO<sub>2</sub> for photocatalytic oxidation of RhB and MB [59,60] and BiVO<sub>4</sub> for photocatalytic oxidation of methyl orange [61]. EuFeO<sub>3</sub> nanoparticles have photo-Fenton-like catalytic activity, as indicated by the efficient decolorization of RhB aqueous solution under visible-light irradiation, and they can be recovered and reused due to their excellent photocatalytic stability [62]. Xu et al. (2014) [63] showed that the addition of Eu<sup>3+</sup> ions on the surface of Bi<sub>2</sub>WO<sub>6</sub> composites enhances the photocatalytic degradation of RhB under visible light irradiation by producing hydroxyl radicals.

Sharmin et al. (2022) [64] synthesized 10% Gd-doped BiFeO<sub>3</sub> nanoparticles (BGFO) via a simple and cost-effective hydrothermal technique at a lower reaction temperature of 160 °C. Following this approach, the synthesized nanoparticles exhibited photocatalytic activity towards the degradation of hazardous industrial pollutants, such as RhB and MB pharmaceutical pollutants such as ciprofloxacin (CIP) and levofloxacin (LFX) under simulated solar irradiation. The photocatalyst BGFO demonstrated 96% and 97% degradation of RhB and MB within 240 and 180 min of solar irradiation, respectively, and about 80% and 79% degradation of CIP and LFX were obtained within 240 min in the same conditions. Similarly, through the hydrothermal method, Sn-Gd<sub>2</sub>O<sub>3</sub> nanomaterial was prepared and mixed with a hot aqueous solution (T > 60 °C) of gelatin polymer, followed by cross-linking, for the efficient reduction of water pollutants [65]. The catalytic activity of Sn-Gd<sub>2</sub>O<sub>3</sub> NPs was analyzed against different dyes, such as 4-nitrophenol (4-NP), 2,6-dinitrophenol (2,6-DNP), 2-nitrophenol (2-NP), MB, methyl orange (MO) and congo red, the presence of a strong reducing agent, NaBH<sub>4</sub>. These latter two anionic azo dyes are used as indicators as well as in the food, textile, paper and pulp, cotton, silk, plastic, cosmetic, pharmaceutical, rubber, printing, and wool industries [66]. Therefore, this scientific approach has led to the fabrication of a new hydrogel nanocomposite for the removal of water pollutants, especially in the reduction of the activity of industrial dyes. Composites of Bi<sub>2</sub>MoO<sub>6</sub> showed an enhanced photodegradation of RhB and TC when doped with Gd and Pt ions, by producing hydroxyl radicals, holes in the valence band (h<sup>+</sup>), and superoxide radicals [67]. Yu et al. (2016) showed that Bi<sub>2</sub>MoO<sub>6</sub> nanoplate crystals perform a better photocatalytic degradation of RhB when doped with Gd<sup>3+</sup> ions, with the production of hydroxyl radicals as a proposed mechanism of action [68]. Wu et al. (2019) [69] showed that the TiO<sub>2</sub> NPs demonstrated an enhanced photocatalytic degradation of MB and RhB when doped with Gd<sup>3+</sup> ion or Gd<sub>2</sub>O<sub>3</sub>.

Vinoshia et al. (2022) [70] showed that zinc ferrite (ZnFe<sub>2</sub>O<sub>4</sub>) nanocrystals doped with dysprosium (Dy) exhibit a photo-Fenton activity against MB with an efficiency of 97.3% within 45 min. This ferrite can act as a magnetic recyclable catalyst even after five cycles with an insignificant lessening of elements.

Liang et al. (2006) [71] showed that Er<sup>3+</sup>-TiO<sub>2</sub> catalysts had higher adsorption equilibrium constants and better adsorption capacity than pure TiO<sub>2</sub>, and the degradation and mineralization of orange I under both UV radiation and visible light were more efficient with Er<sup>3+</sup>-TiO<sub>2</sub> catalyst than with pure TiO<sub>2</sub>.

Tikhanova et al. (2021) [72] showed that the heterojunction h-YbFeO<sub>3</sub>/o-YbFeO<sub>3</sub> photocatalyst demonstrates an enhanced photo-Fenton decolorization of MV under visible light compared to pure o-YbFeO<sub>3</sub>. A novel developed 2.0%Yb/2.0%Er/2.0%Pr-BiW<sub>2</sub>O<sub>6</sub> catalyst could degrade the Congo red dye, TC, RhB, and MB by 90.2%, 52.3%, 95.5%, and



64.6%, respectively, under visible light illumination. The proposed mechanism of action was the promoted reactive oxide species production and photocarrier separation [73].

The addition of  $\text{Ln}_2\text{O}_3$  ( $\text{Ln} = \text{Sm}, \text{Eu}$  or  $\text{Tb}$ ) on the surface of  $\text{BiVO}_4$  composites enhanced the degradation of RhB with respect to the individual composites, by producing superoxide radicals, holes ( $\text{h}^+$ ), and hydroxyl radicals [74]. In the study of [75], the  $\text{Bi}_2\text{WO}_6$  photocatalyst showed enhanced performance in the degradation of RhD when doped with the combination of  $\text{Tb}/\text{Eu}$ ,  $\text{Dy}/\text{Sm}$ , or  $\text{Er}/\text{Nd}$ . The proposed mechanism of action was the production of hydroxyl radicals, holes ( $\text{h}^+$ ), and superoxide radicals.

Among the catalysts discussed, the most promising results for the removal of dyes were obtained with nanocerium doped with  $\text{Cu}$ ,  $\text{Fe}$ ,  $\text{Zr}$ ,  $\text{Dy}$ , or  $\text{La}$ , which achieved a remarkable removal efficiency of over 99% MB [45]. These catalysts demonstrated a high level of effectiveness in degrading and eliminating MB from wastewater, showcasing their potential for applications in water treatment. However, it is important to consider that the performance of catalysts can be influenced by various factors, such as reaction conditions and the specific dye compound being targeted. Optimal results may vary depending on these factors and further exploration and optimization are necessary to discover even more efficient catalysts for MB removal. By improving catalyst design, fine-tuning reaction conditions, and exploring novel materials, it may be possible to achieve even higher removal efficiencies and enhance the overall sustainability and efficiency of water treatment processes.

### 3.3. Degradation of Other Target Pollutants

With the rapid development of industrialization, wastewater has increasingly enriched itself with various substances which often include, in addition to those already extensively discussed above, alkaloids, herbicides, phenols, etc. Unconventional wastewater treatment methods are presented below based on photocatalysis and Fenton-like reaction using REEs for the abatement of these molecules. In the first-ever study using REEs for removing pollutants from aqueous solutions, [33] studied the use of solid compounds of  $\text{Y}(\text{III})$ ,  $\text{La}(\text{III})$ ,  $\text{Ce}(\text{III})$ ,  $\text{Nd}(\text{III})$ ,  $\text{Sm}(\text{III})$ ,  $\text{Gd}(\text{III})$ , and  $\text{Ce}(\text{IV})$  in the form of oxides, hydrous oxides and basic carbonates for the removal of fluoride ions, and only  $\text{Ce}(\text{IV})$  was capable of removing them effectively without a significant dissolution even at pH 2.

Fouad et al. (2021) [76] tried to modify the  $\text{LaFeO}_3$  catalyst with  $\text{Ti}$  ( $\text{Ti-LaFeO}_3$ ) by developing photocatalysis and photo-Fenton processes under UV and visible light for the degradation of carbofuran (CBF). It was observed that about 20% of CBF was degraded by  $\text{H}_2\text{O}_2$  without catalyst loading under UV irradiation. In the presence of UV light and the absence of  $\text{H}_2\text{O}_2$ , the CBF degradation was 59%, which was mainly due to the photocatalysis process induced by the illumination of  $\text{Ti-LaFeO}_3$ . The degradation of CBF was 73% under metal-halide lamp irradiation in the system of  $\text{Ti-LaFeO}_3/\text{H}_2\text{O}_2$ , which confirms the activity of the catalyst under visible light. Moreover, the degradation was improved to 89.5% when this lamp was replaced by UV light. Heterogeneous catalytic wet peroxide oxidation (CWPO) was proposed in this work, aiming to obtain degradation rates and faster mineralization of recalcitrant pollutants like CBF [77]. The results showed that the efficiency of the CWPO process by  $\text{Ti-LaFeO}_3$  is higher than other photocatalytic processes used in the literature for the degradation of CBF. Furthermore, the catalyst could maintain its catalytic activity for five consecutive cycles. In the study of [78], the  $\text{La}$ -doped  $\text{TiO}_2$  photocatalyst could degrade acetone and  $\text{NO}$  under visible light by 38% and 98%, respectively.

Gogoi et al. (2017) [79] used  $\text{Fe}_3\text{O}_4\text{-CeO}_2$  nanocomposite materials as a Fenton-like heterogeneous catalyst for the degradation of catechol.  $\text{Fe}_3\text{O}_4\text{-CeO}_2$  (15 wt%) showed the maximum degradation of catechol compared to the other prepared catalysts. The catalyst could also be recovered and used for five consecutive cycles with excellent catalytic activity. Cerium chloride exhibited radical production in the presence of hydrogen peroxide, as assessed by relaxation of supercoiled plasmid DNA and the production of radical cation of 2,2'-azinobis-(3-ethylbenzthiazoline-6-sulfonic acid), and so it is proposed that cerium is

capable of redox-cycling with peroxide to generate damaging oxygen radicals [80]. Orge et al. (2012) [81] tested ceria and Ce-based mixed oxides (Ce-Sm, Ce-La, and Ce-Zr with different compositions) as catalysts in the ozonation of oxalic acid, aniline, and the textile dye C. I. Reactive Blue 5. CeO<sub>2</sub>-ZrO<sub>2</sub> catalyst with higher than 25 wt.% of ZrO<sub>2</sub> presented the best catalytic oxidation of oxalic acid, which may be related to the larger percentage of the Ce (III) species on their surfaces. On the other hand, the ozonation catalyzed by 25 wt.% of Zr, Sm, or La oxides with Ce oxide or by Ce oxide did not present significant differences. In addition, the association of O<sub>3</sub> and all mentioned catalysts leads to an improved TOC removal from the dye and almost complete mineralization in all cases after about two hours. The highest mineralization rate of aniline was achieved by CeO<sub>2</sub> and Ce<sub>0.75</sub>Zr<sub>0.25</sub>O<sub>2</sub> with the latter being the sample with the largest amount of oxygen vacancies number in its structure. Cerium nanotubes catalysts (CeNTs) doped with different amounts of Nb<sub>2</sub>O<sub>5</sub> (0–10 wt.%) were used for the catalytic reduction of NO<sub>x</sub> with NH<sub>3</sub> (NH<sub>3</sub>-SCR) in the presence of CH<sub>2</sub>Cl<sub>2</sub>. The 10 wt.% Nb-CeNTs catalyst presented the best oxidation of NH<sub>3</sub>-SCR and degradation efficiency of CH<sub>2</sub>Cl<sub>2</sub> among the prepared catalysts, due to its abundant surface oxygen species and acid sites, superior redox capability, the interaction between Nb and Ce, higher ratio of Nb<sup>4+</sup>/(Nb<sup>5+</sup>+ Nb<sup>4+</sup>) and Ce<sup>3+</sup>/(Ce<sup>3+</sup>+ Ce<sup>4+</sup>), and the special tubular structure of the Ce nanotube [82].

A magnetic nanoscaled Fe<sub>3</sub>O<sub>4</sub>/CeO<sub>2</sub> composite can degrade 4-chlorophenol and be reused for six successive cycles [83].

A ZnO nanoparticle doped with 2% Ce can catalyze the oxidation of cyanide and subsequently of cyanate as well under UV-A light or natural sunlight [84].

Sharma et al. (2016) [44] doped cobalt ferrite (CoFe<sub>2</sub>O<sub>4</sub>) with La or Ce and observed an enhancement in its photo-Fenton degradation properties of various organic pollutants using two different inorganic oxidants: hydrogen peroxide (H<sub>2</sub>O<sub>2</sub>) and potassium peroxymonosulphate (KHSO<sub>5</sub>), with respect to pure cobalt ferrite. The doped catalyst could also be reused in wastewater treatment without a decline in its catalytic activity due to its chemical stability.

Samarium-doped ZnO nanorods (Sm/ZNRs) can exhibit a higher photocatalytic degradation of phenol aqueous solution under visible light irradiation than that of the pure ZNRs due to their high charge separation efficiency and OH• generation ability. These nanorods could also be reused for more cycles [85].

Cymes et al. (2020) [86] doped cryptomelane with europium via either co-precipitation or ion exchange in order to promote the catalytic oxidation of ethanol. Eu-doping by co-precipitation generally improves catalytically advantageous physical and chemical properties whereas Eu-doping by ion exchange shows deleterious effects.

Composites of Bi<sub>2</sub>MoO<sub>6</sub> showed an enhanced photodegradation of 4-Chlorophenol when doped with Gd and Pt ions, by producing hydroxyl radicals, holes in the valence band (h<sup>+</sup>), and superoxide radicals [49]. In the study of [63], the Bi<sub>2</sub>WO<sub>6</sub> photocatalyst showed enhanced performance in the degradation of phenol when doped with the combination of Tb/Eu, Dy/Sm, or Er/Nd. The proposed mechanism of action was the production of hydroxyl radicals, holes (h<sup>+</sup>), and superoxide radicals.

Table 2 shows which REEs have been studied for photocatalysis and which for Fenton-like catalysis.

Tables 3–5 below summarize all the catalyst-doped REEs divided and ordered according to publication date.

**Table 3.** REE catalysts used for pharmaceutical degradation.

Catalyst Doped REE	Target	Dose of Catalyst	Dose of Target	Time (min)	Conditions	Proposed Mechanism	Removal (%)	Reference
LaFeO <sub>3</sub>	Sulfamethoxazole	1.4 g/L	3 mg/L	120	pH = 6.48, T = 30 °C	Production of •OH and superoxide radicals (O <sub>2</sub> <sup>-</sup> /HOO)	100%	[31]
LaFeO <sub>3</sub> /MIL-125-NH <sub>2</sub>	Carbamazepine (CBZ) and Caffeine (CAF)	250 mg/L	5 mg/L CBZ and 1 mg/L CAF	60	Visible light	Production of •OH and O <sub>2</sub> <sup>-</sup>	74% CBZ 87% CAF	[32]
LaFeO <sub>3</sub> /lignin-biochar (LFO/LG)	Ofloxacin (OFX)	250 mg/L	30 mg/L	75	Visible light, addition of H <sub>2</sub> O <sub>2</sub>	Production of •OH	95.60%	[33]
CeO <sub>2</sub> /C gas diffusion electrode (GDE)	Dipyrene	-	100 mg/L	20	-	Production of •OH	100%	[34]
FeCeO <sub>x</sub>	Diclofenac	0.5 g/L	20 mg/L	40	pH = 5, addition of H <sub>2</sub> O <sub>2</sub> , ambient temperature	Production of •OH	83%	[35]
CeO <sub>2</sub> nanosheets doped with Fe	Salicylic acid	250 mg/L	50 mg/L	120	Addition of H <sub>2</sub> O <sub>2</sub> , pH = 4, T = 55 °C	Production of superoxide radicals (O <sub>2</sub> <sup>-</sup> /HOO)	96% by 2wt% Fe-CeO <sub>2</sub>	[36]
CeO <sub>x</sub> modified graphite felt	Carbamazepine	-	10 mg/L	60	pH = 5, T = 25 °C	Production of •OH	69.40%	[37]
Sponge-like structure of Co- and Gd-modified biochar (MBC)	Ciprofloxacin (CIP)/Tetracycline (TC)	1.1 g/L	20 mg/L	180	pH = 9	-	99% of CIP or TC	[38]
Er <sub>2</sub> FeSbO <sub>7</sub> /BiTiSbO <sub>6</sub> heterojunction (EBH) catalyst	Enrofloxacin (ENR)	0.75 g/L	0.025 mM	150	Visible light, T = 20 °C,	Production of •OH	99.16%	[39]
FeOCl doped with Y or LA	Ibuprofen	0.5 g/L	5 mg/L	20	Neutral pH, addition of H <sub>2</sub> O <sub>2</sub> , room temperature, dark	Production of •OH	84–82% by 0.9wt% FeOCl/La and 1.2wt% FeOCl/Y, respectively	[40]
Gd doped BiFeO <sub>3</sub> nanoparticles (BGFO)	Ciprofloxacin (CIP)/Levofloxacin (LFX)	-	-	240	Solar illumination	Production of O <sub>2</sub> <sup>-</sup>	80%/79%	[64]

**Table 4.** REE catalysts used for dyes degradation.

Catalyst Doped REE	Target	Dose of Catalyst	Dose of Target	Time (min)	Conditions	Proposed Mechanism	Removal (%)	Reference
La-Fe MMT	Rhodamine B (RhB)/Methylene Blue (MB)	1 g/L	100 mg/L	60	Neutral pH, addition of H <sub>2</sub> O <sub>2</sub>	Production of •OH	97% MB 96% RhB	[40]
Tungsten oxide composites (WO <sub>3</sub> ) doped with La, Gd, or Er	Organic dyes	300 mg/L	-	90	Visible light,	Production of O <sub>2</sub> <sup>-</sup>	98% for MB and >90% for MT, MO, TC and CV by 2% Gd-doped WO <sub>3</sub>	[42]
FeAl/Ce-Mts and FeAl/La-Mts	Reactive Blue 19	0.5 g/L	0.12 mM	180	Sunlight, addition of H <sub>2</sub> O <sub>2</sub> , pH = 3.0	Production of •OH	100% by FeAl/Ce1.0-Mt and 99.7% with FeAl/La1.0-Mt	[43]

Table 4. Cont.

Catalyst Doped REE	Target	Dose of Catalyst	Dose of Target	Time (min)	Conditions	Proposed Mechanism	Removal (%)	Reference
CoFe <sub>2</sub> O <sub>4</sub> doped with La or Ce	Remazol black 5, remazol brilliant yellow, <i>o</i> -nitrophenol, <i>m</i> -nitrophenol (MNP) and <i>p</i> -nitrophenol	0.5 g/L	-	ott-30	Visible light, room temperature, pH = 2.5, addition of H <sub>2</sub> O <sub>2</sub>	Production of •OH	-	[44]
Nanoceria doped with Cu, Fe, Zr, Dy or La	MB	80 mg/L	55.2 mg/L	420	pH = 9.6, T = 27 °C, UV light	Production of •OH	>99% by CuO/CeO <sub>2</sub>	[45]
Cu-Mn/CeO <sub>2</sub> /SBA-15	RhB	200 mg/L	2 g/L	210	pH = 7.0, addition of H <sub>2</sub> O <sub>2</sub> , atmospheric pressure and constant temperature	Production of •OH	0.99	[46]
Ce <sub>4</sub> <sup>+</sup> -TiO <sub>2</sub> sol and nanocrystallites	Brilliant red dye (X-3B)	1 g/L	100 mg/L	120	Visible light	Production of •OH and O <sub>2</sub> <sup>-</sup>	83.1% by Ce <sub>4</sub> <sup>+</sup> -TiO <sub>2</sub> nanocrystallines and 99.9% by Ce <sub>4</sub> <sup>+</sup> -TiO <sub>2</sub> sol	[47]
Cu/zeolite Y	Congo red (CR)	1 g/L	0.143 mM	150	Addition of H <sub>2</sub> O <sub>2</sub> , pH = 7.0	Production of •OH	93.58% by 7.5wt% Cu	[48]
PrFeO <sub>3</sub>	Methyl violet (MV)	250 mg/L	23.2 mg/L	60	Addition of H <sub>2</sub> O <sub>2</sub> , visible light	Production of •OH	-	[50]
PrFeO <sub>3</sub> /CeO <sub>2</sub> -based nanocomposites	MV	250 mg/L	23.2 mg/L	30	Visible light, addition of H <sub>2</sub> O <sub>2</sub>	Production of •OH	80.1% by 9 wt% CeO <sub>2</sub>	[51]
Pr-CdWO <sub>4</sub> NPs	Remazol Black B	350 mg/L	100 mg/L	100	pH = 3.0, T = 25 °C, addition of enhancers	Production of •OH	93.90%	[52]
ZnO nanoneedles doped with Nd	MB	5 g/L	10 <sup>-5</sup> M	300	UV light	Production of O <sub>2</sub> <sup>-</sup>	92% by 1% Nd-doped ZnO	[53]
LaFeO <sub>3</sub> perovskites doped with Eu, Gd, Dy, or Nd	Safranin-O and remazol brilliant yellow	0.5 g/L	15 mg/L SO and 60 mg/L RBY	20, 35, 35, 20	Visible light, pH = 2.0, adding H <sub>2</sub> O <sub>2</sub>	Production of •OH	More than 90%	[54]
ZnFe <sub>2</sub> O <sub>4</sub> nanocrystals doped with Sm	MB	0.1 g/L	1 mg/L	60	Visible light	Production of •OH	65% by 2 wt% Sm	[55]
Sm doped CeO <sub>2</sub> nanoparticles	Rose bengal dye	1 g/L	5 mg/L	90	UV light	Production of •OH	84% by 4 wt% Sm and 89% by 6 wt% Sm	[56]
Eu-N co-doped TiO <sub>2</sub> /Sepiolite NCs	Orange G	0.8 g/L	10 mg/L	540	Visible light, pH = 3.0	Production of •OH	More than 98% by 0.6 wt% Eu	[58]
Eu <sup>3+</sup> -TiO <sub>2</sub>	RhB	2 g/L	10 <sup>-5</sup> M	30	UV light	Formation of a complex between the doped lanthanide ions and substrates	96%	[59]
Eu <sup>2+</sup> -TiO <sub>3</sub>	MB	0.125 M	2 × 10 <sup>-5</sup> M	60	UV light, pH = 8.3	Induced surface plasmon resonances	-	[60]

Table 4. Cont.

Catalyst Doped REE	Target	Dose of Catalyst	Dose of Target	Time (min)	Conditions	Proposed Mechanism	Removal (%)	Reference
Eu <sup>2+</sup> , <sup>3+</sup> -BiVO <sub>4</sub>	Methyl orange (MO)	2 g/L	10 mg/L	180	Visible light	Trapping of photogenerated electrons in the catalyst by Eu dopant	93.6% by 1.46 wt% Eu	[61]
EuFeO <sub>3</sub> NPs	RhB	1 g/L	5 mg/L	180	Visible light, room temperature, addition of H <sub>2</sub> O <sub>2</sub>	Production of •OH	71%	[62]
Gd doped BiFeO <sub>3</sub> NPs (BGFO)	RhB/MB	-	-	240/180	Solar illumination	Production of O <sub>2</sub> <sup>-</sup>	96%/97%	[64]
Sn-Gd <sub>2</sub> O <sub>3</sub> NPs	4-NP, 2,6-DNP, 2-NP, MB, MO and CR	8 g/L	0.07 mM	18	Addition of NaBH <sub>4</sub>	Electron transfer from the catalyst to the dye	-	[65]
ZnFe <sub>2</sub> O <sub>4</sub> nanocrystals doped with Dy	MB	1 g/L	20 mg/L	45	Visible light, addition of H <sub>2</sub> O <sub>2</sub>	Production of •OH	97.30%	[66]
Er <sup>3+</sup> -TiO <sub>2</sub>	Orange I	1 g/L	6 × 10 <sup>-5</sup> M	60	T = 25 °C, UV light or visible light, pH = 7.0	Production of •OH	About 100% under UV and about 80% under visible light by 1.5 wt% Er	[70]
Heterojunction h-YbFeO <sub>3</sub> /o-YbFeO <sub>3</sub>	MV	125 mg/L	0.25 mM	180	Visible light, addition of H <sub>2</sub> O <sub>2</sub>	Production of •OH	64%	[72]
Yb/Er/Pr-Bi <sub>2</sub> WO <sub>6</sub> catalyst	CR/TC/RhB/MB	1 g/L	-	60	Visible light	Reactive oxide species production and photocarrier separation	90.2%/52.3%/95.5%/64.6%	[73]
BiVO <sub>4</sub> composites doped with Ln <sub>2</sub> O <sub>3</sub> (Ln = Sm, Eu, or Tb)	RhB	1 g/L	10 mmol/L	210	Visible light, 25 °C	Production of •O <sub>2</sub> <sup>-</sup> , holes in the valence band (h <sup>+</sup> ), and •OH	55.1%, 51.8%, and 57.3% by 2% Sm <sub>2</sub> O <sub>3</sub> /BiVO <sub>4</sub> , 2% Eu <sub>2</sub> O <sub>3</sub> /BiVO <sub>4</sub> , and 10% Tb <sub>2</sub> O <sub>3</sub> /BiVO <sub>4</sub> , respectively	[74]
Y-Bi <sub>2</sub> WO <sub>6</sub> photocatalyst	RhB	1 g/L	0.01 mM	240	Visible light	Production of holes (h <sup>+</sup> ) and O <sub>2</sub> <sup>-</sup>	85% by 1% Y-Bi <sub>2</sub> WO <sub>6</sub>	[49]
Gd/Pt-Bi <sub>2</sub> MoO <sub>6</sub> composites	RhB/TCs	1 g/L	12 mg/L RhB/20 mg/L TCs	80 for RhB and 90 for TCs	UV visible light	Production of •O <sub>2</sub> <sup>-</sup> , holes in the valence band (h <sup>+</sup> ), and •OH	95% of RhB and 77.6% of TCs by 2%Gd/2%Pt-Bi <sub>2</sub> MoO <sub>6</sub>	[67]
Eu-doped Bi <sub>2</sub> WO <sub>6</sub> composites	RhB	1 g/L	10 mg/L	60	Visible light, 25 °C, addition of H <sub>2</sub> O <sub>2</sub>	Production of OH radicals	98%	[63]
Ln1/Ln2 co-doped Bi <sub>2</sub> MoO <sub>6</sub> photocatalysts (Ln1/Ln2 = Tb/Eu, Dy/Sm, Er/Nd)	RhB	1 g/L	12 mg/L	240	UV visible light	Production of OH, holes (h <sup>+</sup> ) and superoxide radicals O <sub>2</sub> <sup>-</sup>	95.9% by 3%Tb/3%Eu, 98.5% by 3%Dy/3%Sm and 91.6% by 2%Er/2%Nd	[75]
Gd <sup>3+</sup> doped Bi <sub>2</sub> MoO <sub>6</sub> nanoplate crystals	RhB	0.5 g/L	20 mg/L	10	Visible light, 20 °C	Production of OH and holes (h <sup>+</sup> )	84% by 6%Gd/Bi <sub>2</sub> MoO <sub>6</sub>	[68]

Table 4. Cont.

Catalyst Doped REE	Target	Dose of Catalyst	Dose of Target	Time (min)	Conditions	Proposed Mechanism	Removal (%)	Reference
Gd <sup>3+</sup> /TiO <sub>2</sub> and Gd <sub>2</sub> O <sub>3</sub> /TiO <sub>2</sub> NPs	MV/RhB	0.2 g/L for MV and 0.1 mg/L for RhB	25 mg/L/30 mg/L	60	UV visible light	Production of •O <sub>2</sub> <sup>-</sup> , holes in the valence band (h <sup>+</sup> ), and •OH	97.9% by 2.5% Gd <sup>3+</sup> /TiO <sub>2</sub>	[69]
Sm-doped Bi <sub>2</sub> MoO <sub>6</sub> photocatalysts	RhB	0.2 g/L	5 mg/L	50	Visible light	Production of •O <sub>2</sub> <sup>2-</sup> and holes (h <sup>+</sup> )	89% by 0.8% Sm-doped Bi <sub>2</sub> MoO <sub>6</sub>	[57]

Table 5. REE catalysts used for herbicide, alkaloid, cyanide, organic acid, and phenol degradation.

Catalyst Doped REE	Target	Dose of Catalyst	Dose of Target	Time (min)	Conditions	Proposed Mechanism	Removal (%)	Reference
Ti-LaFeO <sub>3</sub>	Carbofuran	700 mg/L	7 mg/L	180	Adding H <sub>2</sub> O <sub>2</sub> , pH = 3.0	Production of •OH	91%	[76]
Ti-substituted LaFeO <sub>3</sub>	4-Chlorophenol	0.5 g/L	25 mg/L	-	Circumneutral pH, ambient atmospheric pressure and temperature, UV-A light, addition of H <sub>2</sub> O <sub>2</sub>	Production of •OH	100% by 3.2% Ti	[77]
Fe <sub>3</sub> O <sub>4</sub> -CeO <sub>2</sub>	Catechol	1 g/L	10 mg/L	60	Adding H <sub>2</sub> O <sub>2</sub> , room temperature, pH = 2.4	Production of ROS	100% by Fe <sub>3</sub> O <sub>4</sub> -CeO <sub>2</sub> (15 wt%)	[79]
Ce-Sm, Ce-La, Ce-Zr	Oxalic acid/Aniline/C.I. Reactive Blue 5	-	C0,oxalic acid = C0,aniline = 1 mM, C0,dye = 50 mg L <sup>-1</sup>	180/30/15	pH0,oxalic acid ≈ 3.0, pH0, aniline ≈ 6.5, pH0, dye ≈ 5.5, constant gas (oxygen + ozone) flow rate and constant inlet ozone concentration, 25 °C	Production of •OH	100% of oxalic acid with more than 25% of Sm, La or Zr/100% of aniline by Ce <sub>0.75</sub> Zr <sub>0.25</sub> O <sub>2</sub> /100% by Ce <sub>0.75</sub> Zr <sub>0.25</sub> O <sub>2</sub>	[80]
Fe <sub>3</sub> O <sub>4</sub> /CeO <sub>2</sub> composite	4-Chlorophenol	2 g/L	0.78 mM	90	Addition of H <sub>2</sub> O <sub>2</sub> , T = 30 °C, pH = 3.0	Production of •OH	100%	[81]
ZnO nanoparticles doped with Ce	Cyanide	4 g/L	-	60	UV-A light or natural sunlight, pH = 12.5	Production of •OH	-	[84]
Sm/ZNRs	Phenol	1 g/L	20 mg/L	480	Visible light, room temperature	Production of •OH radicals	89.5% by 1 wt% Sm/ZNRs	[85]
Cryptomelane doped with Eu	Ethanol	50 mg	-	-	Dark, T = 175–200 °C	Production of O <sub>2</sub> <sup>-</sup>	100%	[86]
Cerium nanotubes catalysts (CeNTs)	NOx	-	600 mg/L	600	Addition of CH <sub>2</sub> Cl <sub>2</sub> , 200 °C	Production of •OH	100% by 10% Nb-CeNTs	[82]
Gd/Pt-Bi <sub>2</sub> MoO <sub>6</sub> composites	4-Chlorophenol	1 g/L	15 mg/L	300	UV visible light	Production of •O <sub>2</sub> <sup>-</sup> , holes in the valence band (h <sup>+</sup> ), and •OH	80% by 2%Gd/2%Pt-Bi <sub>2</sub> MoO <sub>6</sub>	[49]

Table 5. Cont.

Catalyst Doped REE	Target	Dose of Catalyst	Dose of Target	Time (min)	Conditions	Proposed Mechanism	Removal (%)	Reference
Ln1/Ln2 co-doped Bi <sub>2</sub> MoO <sub>6</sub> photocatalysts (Ln1/Ln2 = Tb/Eu, Dy/Sm, Er/Nd)	Phenol	1 g/L	15 mg/L	300	UV visible light	Production of •O <sub>2</sub> <sup>-</sup> , holes in the valence band (h <sup>+</sup> ), and •OH	76.2%, 79.1% and 70.7% by 3%Tb/3%Eu, 3%Dy/3%Sm and 2%Er/2%Nd, respectively	[75]
La-doped TiO <sub>2</sub> photocatalyst	Acetone/NO	-	1000 ppb/500 ppb	30	UV visible light	Production of •O <sub>2</sub> <sup>-</sup> and •OH	38% of acetone and 98% of NO by 0.5%La-TiO <sub>2</sub>	[78]

#### 4. Potential Environmental Impacts of REE Catalysts

As for the use of REEs in AOPs, different perspectives are to be considered. Further improvement needs to be implemented in water treatments; as of now, several methods have been adopted that increase efficiency and provide better handling of waste, such as Fenton-like oxidation processes [87]. Studies focused on the use of lanthanides have demonstrated an improvement in wastewater treatments, as their use can produce on average 30% less sludge compared to other alternatives such as iron and aluminum [88]. The use of REEs could represent an alternative for reducing wastelands generated by sludge [88] and improving the removal of organic pollutants by enhancing photocatalytic activity [23].

Moreover, care should be taken to avoid the loss and transfer of particles into the environment, contributing to the anthropogenic input of REEs. The authors of [89] found that the mixture of lanthanides used in wastewater treatment had an antagonistic behavior, which could reduce their environmental impact. However, up to now, the knowledge of the toxicity of REEs is very limited, as the environmental fate is highly dependent on the system, such as the presence of organic matter, pH, and presence of cations [90] which influence the speciation, which, by extension influences the bioaccumulation and bioavailability. Because of the lack of knowledge regarding the potential effects of REEs, the regulation for the discharge of REEs is still lacking. In contrast, many restrictions regarding the presence of organic pollutants have been applied globally [91].

#### 5. Conclusions

The study of REEs for their potential use in removing toxic organic compounds from aqueous solutions is a relatively recent field, with the first publication on this topic occurring only 28 years ago. Among the REEs, cerium has been extensively studied for its photo Fenton-like catalytic activity against organic pollutants, followed by lanthanum. However, the remaining REEs have received little attention, with five of them having never been studied in this context.

REEs have been shown to be promising for removing hazardous organic compounds from aqueous solutions, such as wastewater. The effectiveness of REEs in this regard depends mainly on the presence of oxygen vacancies and the concentration of REE ions in the catalysts. Specifically, the metal oxide surfaces promote the decomposition of hydrogen peroxide, which leads to the formation of hydroxide species responsible for the degradation of organic compounds.

Moreover, AOPs, which include REE-combined catalysts and other parameters, should be chosen based on the nature of the contaminants and the acid-base properties of the wastewater to be treated.

Due to their exceptional properties, REEs have the potential to revolutionize wastewater treatment. However, achieving the production of clean water without generating traces of persistent toxins remains a challenging goal.

**Author Contributions:** L.S.: Conceptualization, Data Curation, Writing—original draft. A.A.B.: Conceptualization, Data Curation, Writing—original draft. E.G.P.S.: Writing—original draft. A.S.: Data Curation, Writing—original draft, Supervision. M.S.: Data Curation. M.G.: Funding acquisition, data curation, and writing—review & editing. M.T.: Funding acquisition, data curation, and writing—review & editing. D.D.B.: Data curation. M.C.: Data Curation—original draft revision. V.R.S.: Conceptualization—data curation. G.L. (Giusy Lofrano): Supervision, Writing—original draft. G.L. (Giovanni Libralato): Writing—original draft, Supervision, Funding acquisition. All authors have read and agreed to the published version of the manuscript.

**Funding:** Funding for this project has been provided through multiple sources including the European Union’s Horizon 2020 research and innovation program under the Marie Skłodowska-Curie grant agreement No. 857989. Additionally, support has been received from NBFC to the University of Palermo Institute, which is funded by the Italian Ministry of University and Research, PNRR, Missione 4 Componente 2, “Dalla ricerca all’impresa”, Investimento 1.4, Project CN00000033.

**Data Availability Statement:** Not applicable.

**Conflicts of Interest:** The authors state that the research was carried out without any potential conflicts of interest arising from commercial or financial relationships.

## References

1. Lofrano, G.; Libralato, G.; Casaburi, A.; Siciliano, A.; Iannece, P.; Guida, M.; Pucci, L.; Dentice, E.; Carotenuto, M. Municipal wastewater spiramycin removal by conventional treatments and heterogeneous photocatalysis. *Sci. Total Environ.* **2018**, *624*, 461–469. [[CrossRef](#)]
2. Priya, A.K.; Gnanasekaran, L.; Rajendran, S.; Qin, J.; Vasseghian, Y. Occurrences and removal of pharmaceutical and personal care products from aquatic systems using advanced treatment—A review. *Environ. Res.* **2022**, *204*, 112298. [[CrossRef](#)] [[PubMed](#)]
3. Rout, P.R.; Zhang, T.C.; Bhunia, P.; Surampalli, R.Y. Treatment technologies for emerging contaminants in wastewater treatment plants: A review. *Sci. Total Environ.* **2021**, *753*, 141990. [[CrossRef](#)] [[PubMed](#)]
4. Lofrano, G.; Libralato, G.; Carotenuto, M.; Guida, M.; Inglese, M.; Siciliano, A.; Meriç, S. Emerging concern from short-term textile leaching: A preliminary ecotoxicological survey. *Bull. Environ. Contam. Toxicol.* **2016**, *97*, 646–652. [[CrossRef](#)] [[PubMed](#)]
5. Ugwu, E.I.; Karri, R.R.; Nnaji, C.C.; John, J.; Padmanaban, V.; Othmani, A.; Ikechukwu, E.L.; Helal, W.M. Application of green nanocomposites in removal of toxic chemicals, heavy metals, radioactive materials, and pesticides from aquatic water bodies. In *Sustainable Nanotechnology for Environmental Remediation*; Elsevier: Amsterdam, The Netherlands, 2022; pp. 321–346.
6. Karri, R.R.; Ravindran, G.; Dehghani, M.H. Wastewater—Sources, toxicity, and their consequences to human health. In *Soft Computing Techniques in Solid Waste and Wastewater Management*; Elsevier: Amsterdam, The Netherlands, 2021; pp. 3–33.
7. Pedrazzani, R.; Bertanza, G.; Brnardić, I.; Cetecioglu, Z.; Dries, J.; Dvarionienė, J.; García-Fernández, A.J.; Langenhoff, A.; Libralato, G.; Lofrano, G. Opinion paper about organic trace pollutants in wastewater: Toxicity assessment in a European perspective. *Sci. Total Environ.* **2019**, *651*, 3202–3221. [[CrossRef](#)] [[PubMed](#)]
8. Werkneh, A.A.; Rene, E.R. Applications of nanotechnology and biotechnology for sustainable water and wastewater treatment. In *Water and Wastewater Treatment Technologies*; Springer: Berlin/Heidelberg, Germany, 2019; pp. 405–430.
9. Andreozzi, R.; Caprio, V.; Insola, A.; Marotta, R. Advanced oxidation processes (AOP) for water purification and recovery. *Catal. Today* **1999**, *53*, 51–59. [[CrossRef](#)]
10. Spasiano, D.; Siciliano, A.; Race, M.; Marotta, R.; Guida, M.; Andreozzi, R.; Pirozzi, F. Biodegradation, ecotoxicity and UV<sub>254</sub>/H<sub>2</sub>O<sub>2</sub> treatment of imidazole, 1-methyl-imidazole and N, N'-alkyl-imidazolium chlorides in water. *Water Res.* **2016**, *106*, 450–460. [[CrossRef](#)] [[PubMed](#)]
11. Lofrano, G.; Rizzo, L.; Grassi, M.; Belgiorno, V. Advanced oxidation of catechol: A comparison among photocatalysis, Fenton and photo-Fenton processes. *Desalination* **2009**, *249*, 878–883. [[CrossRef](#)]
12. Wang, S. A comparative study of Fenton and Fenton-like reaction kinetics in decolourisation of wastewater. *Dye Pigment* **2008**, *76*, 714–720. [[CrossRef](#)]
13. Wang, N.; Zheng, T.; Zhang, G.; Wang, P. A review on Fenton-like processes for organic wastewater treatment. *J. Environ. Chem. Eng.* **2016**, *4*, 762–787. [[CrossRef](#)]
14. Kuang, J.C. Characteristics of Electron Structure and 4f Orbital of Rare Earths and Their Reinforcement of Wastewater Degradation. *Adv. Mater. Res.* **2014**, *1022*, 72–75. [[CrossRef](#)]
15. Atalay, S.; Ersöz, G. *Novel Catalysts in Advanced Oxidation of Organic Pollutants*; Springer: Berlin/Heidelberg, Germany, 2016.
16. Acharya, B.K.; Pathak, H.; Mohana, S.; Shouche, Y.; Singh, V.; Madamwar, D. Kinetic modelling and microbial community assessment of anaerobic biphasic fixed film bioreactor treating distillery spent wash. *Water Res.* **2011**, *45*, 4248–4259. [[CrossRef](#)] [[PubMed](#)]
17. Kumar, V.; Shah, M.P. Advanced oxidation processes for complex wastewater treatment. In *Advanced Oxidation Processes for Effluent Treatment Plants*; Elsevier: Amsterdam, The Netherlands, 2021; pp. 1–31.



18. Oturan, M.A.; Aaron, J.-J. Advanced oxidation processes in water/wastewater treatment: Principles and applications. A review. *Crit. Rev. Environ. Sci. Technol.* **2014**, *44*, 2577–2641. [[CrossRef](#)]
19. Zhang, N.; Chen, J.; Fang, Z.; Tsang, E.P. Ceria accelerated nanoscale zerovalent iron assisted heterogenous Fenton oxidation of tetracycline. *Chem. Eng. J.* **2019**, *369*, 588–599. [[CrossRef](#)]
20. Oliverio, M.; Nardi, M.; Costanzo, P.; Di Gioia, M.L.; Procopio, A. Erbium salts as non-toxic catalysts compatible with alternative reaction media. *Sustainability* **2018**, *10*, 721. [[CrossRef](#)]
21. Zinatloo-Ajabshir, S.; Emsaki, M.; Hosseinzadeh, G. Innovative construction of a novel lanthanide cerate nanostructured photocatalyst for efficient treatment of contaminated water under sunlight. *J. Colloid Interface Sci.* **2022**, *619*, 1–13. [[CrossRef](#)] [[PubMed](#)]
22. Ambaye, T.G.; Vaccari, M.; Castro, F.D.; Prasad, S.; Rtimi, S. Emerging technologies for the recovery of rare earth elements (REEs) from the end-of-life electronic wastes: A review on progress, challenges, and perspectives. *Environ. Sci. Pollut. Res.* **2020**, *27*, 36052–36074. [[CrossRef](#)] [[PubMed](#)]
23. Chan, S.H.S.; Yeong Wu, T.; Juan, J.C.; Teh, C.Y. Recent developments of metal oxide semiconductors as photocatalysts in advanced oxidation processes (AOPs) for treatment of dye waste-water. *J. Chem. Technol. Biotechnol.* **2011**, *86*, 1130–1158. [[CrossRef](#)]
24. Bokare, A.D.; Choi, W. Review of iron-free Fenton-like systems for activating H<sub>2</sub>O<sub>2</sub> in advanced oxidation processes. *J. Hazard. Mater.* **2014**, *275*, 121–135. [[CrossRef](#)]
25. Onozuka, K.; Kawakami, Y.; Imai, H.; Yokoi, T.; Tatsumi, T.; Kondo, J. Perovskite-type La<sub>2</sub>Ti<sub>2</sub>O<sub>7</sub> mesoporous photocatalyst. *J. Solid State Chem.* **2012**, *192*, 87–92. [[CrossRef](#)]
26. Assila, O.; Barros, Ó.; Fonseca, A.M.; Parpot, P.; Soares, O.S.; Pereira, M.F.; Zerrouq, F.; Kherbeche, A.; Rombi, E.; Tavares, T. Degradation of pollutants in water by Fenton-like oxidation over LaFe-catalysts: Optimization by experimental design. *Microporous Mesoporous Mater.* **2023**, *349*, 112422. [[CrossRef](#)]
27. Song, J.; Ma, N.; Chen, W.; Chen, J.; Dai, Q. Insights into mechanism of catalytic ozonation of cinnamyl alcohol over core-shell Fe<sub>3</sub>O<sub>4</sub>@SiO<sub>2</sub>@La<sub>2</sub>O<sub>3</sub> catalyst. *Sep. Purif. Technol.* **2022**, *282*, 119969. [[CrossRef](#)]
28. Tokunaga, S.; Haron, M.J.; Wasay, S.A.; Wong, K.F.; Laosangthum, K.; Uchiumi, A. Removal of fluoride ions from aqueous solutions by multivalent metal compounds. *Int. J. Environ. Stud.* **1995**, *48*, 17–28. [[CrossRef](#)]
29. Liu, S. Electronic structure of rare earth metals. *Handb. Phys. Chem. Rare Earths* **1978**, *1*, 233–335.
30. Been, E.; Lee, W.-S.; Hwang, H.Y.; Cui, Y.; Zaanen, J.; Devereaux, T.; Moritz, B.; Jia, C. Electronic structure trends across the rare-earth series in superconducting infinite-layer nickelates. *Phys. Rev. X* **2021**, *11*, 011050. [[CrossRef](#)]
31. Nie, Y.; Zhang, L.; Li, Y.-Y.; Hu, C. Enhanced Fenton-like degradation of refractory organic compounds by surface complex formation of LaFeO<sub>3</sub> and H<sub>2</sub>O<sub>2</sub>. *J. Hazard. Mater.* **2015**, *294*, 195–200. [[CrossRef](#)] [[PubMed](#)]
32. Younes, H.A.; Taha, M.; Khaled, R.; Mahmoud, H.M.; Abdelhameed, R.M. Perovskite/metal-organic framework photocatalyst: A novel nominee for eco-friendly uptake of pharmaceuticals from wastewater. *J. Alloys Compd.* **2023**, *930*, 167322. [[CrossRef](#)]
33. Chen, X.; Zhang, M.; Qin, H.; Zhou, J.; Shen, Q.; Wang, K.; Chen, W.; Liu, M.; Li, N. Synergy effect between adsorption and heterogeneous photo-Fenton-like catalysis on LaFeO<sub>3</sub>/lignin-biochar composites for high efficiency degradation of ofloxacin under visible light. *Sep. Purif. Technol.* **2022**, *280*, 119751. [[CrossRef](#)]
34. Assumpção, M.H.M.T.; Moraes, A.; De Souza, R.; Reis, R.M.; Rocha, R.S.; Gaubeur, I.; Calegari, M.L.; Hammer, P.; Lanza, M.R.d.V.; Santos, M.C.d. Degradation of dipyrone via advanced oxidation processes using a cerium nanostructured electrocatalyst material. *Appl. Catal. A Gen.* **2013**, *462*, 256–261. [[CrossRef](#)]
35. Chong, S.; Zhang, G.; Zhang, N.; Liu, Y.; Zhu, J.; Huang, T.; Fang, S. Preparation of FeCeO<sub>x</sub> by ultrasonic impregnation method for heterogeneous Fenton degradation of diclofenac. *Ultrason. Sonochem.* **2016**, *32*, 231–240. [[CrossRef](#)]
36. Wang, W.; Zhu, Q.; Qin, F.; Dai, Q.; Wang, X. Fe doped CeO<sub>2</sub> nanosheets as Fenton-like heterogeneous catalysts for degradation of salicylic acid. *Chem. Eng. J.* **2018**, *333*, 226–239. [[CrossRef](#)]
37. Wang, X.; Jin, Y.; Chen, W.; Zou, R.; Xie, J.; Tang, Y.; Li, X.; Li, L. Electro-catalytic activity of CeO<sub>x</sub> modified graphite felt for carbamazepine degradation via E-peroxone process. *Front. Environ. Sci. Eng.* **2021**, *15*, 122. [[CrossRef](#)]
38. Hu, B.; Tang, Y.; Wang, X.; Wu, L.; Nong, J.; Yang, X.; Guo, J. Cobalt-gadolinium modified biochar as an adsorbent for antibiotics in single and binary systems. *Microchem. J.* **2021**, *166*, 106235. [[CrossRef](#)]
39. Luan, J.; Liu, W.; Yao, Y.; Ma, B.; Niu, B.; Yang, G.; Wei, Z. Synthesis and Property Examination of Er<sub>2</sub>FeSbO<sub>7</sub>/BiTiSbO<sub>6</sub> Heterojunction Composite Catalyst and Light-Catalyzed Retrogradation of Enrofloxacin in Pharmaceutical Waste Water under Visible Light Irradiation. *Materials* **2022**, *15*, 5906. [[CrossRef](#)] [[PubMed](#)]
40. Fida, H.; Zhang, G.; Guo, S.; Naeem, A. Heterogeneous Fenton degradation of organic dyes in batch and fixed bed using La-Fe montmorillonite as catalyst. *J. Colloid Interface Sci.* **2017**, *490*, 859–868. [[CrossRef](#)] [[PubMed](#)]
41. Shi, X.; Cui, C.; Zhang, L.; Zhang, J.; Liu, G. FeOCl/Ln (Ln = La or Y): Efficient photo-Fenton catalysts for ibuprofen degradation. *New J. Chem.* **2019**, *43*, 16273–16280. [[CrossRef](#)]
42. Tahir, M.B.; Sagir, M. Carbon nanodots and rare metals (RM = La, Gd, Er) doped tungsten oxide nanostructures for photocatalytic dyes degradation and hydrogen production. *Sep. Purif. Technol.* **2019**, *209*, 94–102. [[CrossRef](#)]
43. Huang, Z.; Wu, P.; Li, H.; Li, W.; Zhu, Y.; Zhu, N. Synthesis and catalytic properties of La or Ce doped hydroxy-FeAl intercalated montmorillonite used as heterogeneous photo Fenton catalysts under sunlight irradiation. *RSC Adv.* **2014**, *4*, 6500–6507. [[CrossRef](#)]
44. Sharma, R.; Bansal, S.; Singhal, S. Augmenting the catalytic activity of CoFe<sub>2</sub>O<sub>4</sub> by substituting rare earth cations into the spinel structure. *RSC Adv.* **2016**, *6*, 71676–71691. [[CrossRef](#)]

45. Divya, T.; Renuka, N. Modulated heterogeneous Fenton-like activity of 'M' doped nanoceria systems (M = Cu, Fe, Zr, Dy, La): Influence of reduction potential of doped cations. *J. Mol. Catal. A Chem.* **2015**, *408*, 41–47. [[CrossRef](#)]
46. Fan, J.; Jiang, X.; Min, H.; Li, D.; Ran, X.; Zou, L.; Sun, Y.; Li, W.; Yang, J.; Teng, W. Facile preparation of Cu–Mn/CeO<sub>2</sub>/SBA-15 catalysts using ceria as an auxiliary for advanced oxidation processes. *J. Mater. Chem. A* **2014**, *2*, 10654–10661. [[CrossRef](#)]
47. Xie, Y.; Yuan, C. Visible-light responsive cerium ion modified titania sol and nanocrystallites for X-3B dye photodegradation. *Appl. Catal. B Environ.* **2003**, *46*, 251–259. [[CrossRef](#)]
48. Singh, L.; Rekha, P.; Chand, S. Cu-impregnated zeolite Y as highly active and stable heterogeneous Fenton-like catalyst for degradation of Congo red dye. *Sep. Purif. Technol.* **2016**, *170*, 321–336. [[CrossRef](#)]
49. Cao, R.; Huang, H.; Tian, N.; Zhang, Y.; Guo, Y.; Zhang, T. Novel Y doped Bi<sub>2</sub>WO<sub>6</sub> photocatalyst: Hydrothermal fabrication, characterization and enhanced visible-light-driven photocatalytic activity for Rhodamine B degradation and photocurrent generation. *Mater. Charact.* **2015**, *101*, 166–172. [[CrossRef](#)]
50. Seroglazova, A.S.; Popkov, V.I. Synthesis of highly active and visible-light-driven PrFeO<sub>3</sub> photocatalyst using solution combustion approach and succinic acid as fuel. *Nanosyst. Phys. Chem. Math.* **2022**, *13*, 649–654. [[CrossRef](#)]
51. Seroglazova, A.S.; Chebanenko, M.I.; Nevedomskiy, V.N.; Popkov, V.I. Solution combustion synthesis of novel PrFeO<sub>3</sub>/CeO<sub>2</sub> nanocomposite with enhanced photo-Fenton activity under visible light. *Ceram. Int.* **2023**, *49*, 15468–15479. [[CrossRef](#)]
52. Ahmadi, S.; Rahdar, A.; Igwegbe, C.A.; Mortazavi-Derazkola, S.; Banach, A.M.; Rahdar, S.; Singh, A.K.; Rodriguez-Couto, S.; Kyzas, G.Z. Praseodymium-doped cadmium tungstate (CdWO<sub>4</sub>) nanoparticles for dye degradation with sonocatalytic process. *Polyhedron* **2020**, *190*, 114792. [[CrossRef](#)]
53. Yayapao, O.; Thongtem, T.; Phuruangrat, A.; Thongtem, S. Ultrasonic-assisted synthesis of Nd-doped ZnO for photocatalysis. *Mater. Lett.* **2013**, *90*, 83–86. [[CrossRef](#)]
54. Dhiman, M.; Singhal, S. Effect of doping of different rare earth (europium, gadolinium, dysprosium and neodymium) metal ions on structural, optical and photocatalytic properties of LaFeO<sub>3</sub> perovskites. *J. Rare Earths* **2019**, *37*, 1279–1287. [[CrossRef](#)]
55. Keerthana, S.; Yuvakkumar, R.; Kumar, P.S.; Ravi, G.; Velauthapillai, D. Rare earth metal (Sm) doped zinc ferrite (ZnFe<sub>2</sub>O<sub>4</sub>) for improved photocatalytic elimination of toxic dye from aquatic system. *Environ. Res.* **2021**, *197*, 111047. [[CrossRef](#)]
56. Chahal, S.; Rani, N.; Kumar, A.; Kumar, P. Electronic structure and photocatalytic activity of samarium doped cerium oxide nanoparticles for hazardous rose bengal dye degradation. *Vacuum* **2020**, *172*, 109075. [[CrossRef](#)]
57. Wang, M.; You, M.; Guo, P.; Tang, H.; Lv, C.; Zhang, Y.; Zhu, T.; Han, J. Hydrothermal synthesis of Sm-doped Bi<sub>2</sub>MoO<sub>6</sub> and its high photocatalytic performance for the degradation of Rhodamine B. *J. Alloys Compd.* **2017**, *728*, 739–746. [[CrossRef](#)]
58. Zhou, F.; Wang, H.; Zhou, S.; Liu, Y.; Yan, C. Fabrication of europium-nitrogen co-doped TiO<sub>2</sub>/Sepiolite nanocomposites and its improved photocatalytic activity in real wastewater treatment. *Appl. Clay Sci.* **2020**, *197*, 105791. [[CrossRef](#)]
59. Zhang, Y.; Zhang, H.; Xu, Y.; Wang, Y. Europium doped nanocrystalline titanium dioxide: Preparation, phase transformation and photocatalytic properties. *J. Mater. Chem.* **2003**, *13*, 2261–2265. [[CrossRef](#)]
60. Hernández, J.V.; Coste, S.; Murillo, A.G.; Romo, F.C.; Kassiba, A. Effects of metal doping (Cu, Ag, Eu) on the electronic and optical behavior of nanostructured TiO<sub>2</sub>. *J. Alloys Compd.* **2017**, *710*, 355–363. [[CrossRef](#)]
61. Zhang, A.; Zhang, J. Effects of europium doping on the photocatalytic behavior of BiVO<sub>4</sub>. *J. Hazard. Mater.* **2010**, *173*, 265–272. [[CrossRef](#)] [[PubMed](#)]
62. Ju, L.; Chen, Z.; Fang, L.; Dong, W.; Zheng, F.; Shen, M. Sol–gel synthesis and photo-Fenton-like catalytic activity of EuFeO<sub>3</sub> nanoparticles. *J. Am. Ceram. Soc.* **2011**, *94*, 3418–3424. [[CrossRef](#)]
63. Xu, X.; Ge, Y.; Li, B.; Fan, F.; Wang, F. Shape evolution of Eu-doped Bi<sub>2</sub>WO<sub>6</sub> and their photocatalytic properties. *Mater. Res. Bull.* **2014**, *59*, 329–336. [[CrossRef](#)]
64. Sharmin, F.; Basith, M. Highly efficient photocatalytic degradation of hazardous industrial and pharmaceutical pollutants using gadolinium doped BiFeO<sub>3</sub> nanoparticles. *J. Alloys Compd.* **2022**, *901*, 163604. [[CrossRef](#)]
65. Marwani, H.M.; Ahmad, S.; Rahman, M.M. Catalytic reduction of environmental pollutants with biopolymer hydrogel cross-linked gelatin conjugated tin-doped gadolinium oxide nanocomposites. *Gels* **2022**, *8*, 86. [[CrossRef](#)]
66. Ismail, M.; Akhtar, K.; Khan, M.; Kamal, T.; Khan, M.A.; M Asiri, A.; Seo, J.; Khan, S.B. Pollution, toxicity and carcinogenicity of organic dyes and their catalytic bio-remediation. *Curr. Pharm. Des.* **2019**, *25*, 3645–3663. [[CrossRef](#)] [[PubMed](#)]
67. Li, H.; Li, W.; Wang, F.; Liu, X.; Ren, C.; Miao, X. Fabrication of Pt nanoparticles decorated Gd-doped Bi<sub>2</sub>MoO<sub>6</sub> nanosheets: Design, radicals regulating and mechanism of Gd/Pt-Bi<sub>2</sub>MoO<sub>6</sub> photocatalyst. *Appl. Surf. Sci.* **2018**, *427*, 1046–1053. [[CrossRef](#)]
68. Yu, C.; Wu, Z.; Liu, R.; He, H.; Fan, W.; Xue, S. The effects of Gd<sup>3+</sup> doping on the physical structure and photocatalytic performance of Bi<sub>2</sub>MoO<sub>6</sub> nanoplate crystals. *J. Phys. Chem. Solids* **2016**, *93*, 7–13. [[CrossRef](#)]
69. Wu, D.; Li, C.; Zhang, D.; Wang, L.; Zhang, X.; Shi, Z.; Lin, Q. Enhanced photocatalytic activity of Gd<sup>3+</sup> doped TiO<sub>2</sub> and Gd<sub>2</sub>O<sub>3</sub> modified TiO<sub>2</sub> prepared via ball milling method. *J. Rare Earths* **2019**, *37*, 845–852. [[CrossRef](#)]
70. Vinosha, P.A.; Vinsla, J.A.; Madhavan, J.; Devanesan, S.; AlSalhi, M.S.; Nicoletti, M.; Xavier, B. Impact of dysprosium doped (Dy) zinc ferrite (ZnFe<sub>2</sub>O<sub>4</sub>) nanocrystals in photo-fenton exclusion of recalcitrant organic pollutant. *Environ. Res.* **2022**, *203*, 111913. [[CrossRef](#)] [[PubMed](#)]
71. Liang, C.-H.; Hou, M.-F.; Zhou, S.-G.; Li, F.-B.; Liu, C.-S.; Liu, T.-X.; Gao, Y.-X.; Wang, X.-G.; Lü, J.-L. The effect of erbium on the adsorption and photodegradation of orange I in aqueous Er<sup>3+</sup>-TiO<sub>2</sub> suspension. *J. Hazard. Mater.* **2006**, *138*, 471–478. [[CrossRef](#)] [[PubMed](#)]

72. Tikhanova, S.M.; Lebedev, L.A.; Martinson, K.D.; Chebanenko, M.I.; Buryanenko, I.V.; Semenov, V.G.; Nevedomskiy, V.N.; Popkov, V.I. The synthesis of novel heterojunction h-YbFeO<sub>3</sub>/o-YbFeO<sub>3</sub> photocatalyst with enhanced Fenton-like activity under visible-light. *New J. Chem.* **2021**, *45*, 1541–1550. [[CrossRef](#)]
73. Li, X.; Li, W.; Liu, X.; Geng, L.; Fan, H.; Ma, X.; Dong, M.; Qiu, H. The construction of Yb/Er/Pr triple-doped Bi<sub>2</sub>WO<sub>6</sub> superior photocatalyst and the regulation of superoxide and hydroxyl radicals. *Appl. Surf. Sci.* **2022**, *592*, 153311. [[CrossRef](#)]
74. Gu, S.; Li, W.; Bian, Y.; Wang, F.; Li, H.; Liu, X. Highly-visible-light photocatalytic performance derived from a lanthanide self-redox cycle in Ln<sub>2</sub>O<sub>3</sub>/BiVO<sub>4</sub> (Ln: Sm, Eu, Tb) redox heterojunction. *J. Phys. Chem. C* **2016**, *120*, 19242–19251. [[CrossRef](#)]
75. Li, H.; Li, W.; Wang, F.; Liu, X.; Ren, C. Fabrication of two lanthanides co-doped Bi<sub>2</sub>MoO<sub>6</sub> photocatalyst: Selection, design and mechanism of Ln<sub>1</sub>/Ln<sub>2</sub> redox couple for enhancing photocatalytic activity. *Appl. Catal. B Environ.* **2017**, *217*, 378–387. [[CrossRef](#)]
76. Fouad, K.; Alalm, M.G.; Bassyouni, M.; Saleh, M.Y. Optimization of catalytic wet peroxide oxidation of carbofuran by Ti-LaFeO<sub>3</sub> dual photocatalyst. *Environ. Technol. Innov.* **2021**, *23*, 101778. [[CrossRef](#)]
77. Garcia-Muñoz, P.; Lefevre, C.; Robert, D.; Keller, N. Ti-substituted LaFeO<sub>3</sub> perovskite as photoassisted CWPO catalyst for water treatment. *Appl. Catal. B Environ.* **2019**, *248*, 120–128. [[CrossRef](#)]
78. Ho, C.-C.; Kang, F.; Chang, G.-M.; You, S.-J.; Wang, Y.-F. Application of recycled lanthanum-doped TiO<sub>2</sub> immobilized on commercial air filter for visible-light photocatalytic degradation of acetone and NO. *Appl. Surf. Sci.* **2019**, *465*, 31–40. [[CrossRef](#)]
79. Gogoi, A.; Navgire, M.; Sarma, K.C.; Gogoi, P. Fe<sub>3</sub>O<sub>4</sub>-CeO<sub>2</sub> metal oxide nanocomposite as a Fenton-like heterogeneous catalyst for degradation of catechol. *Chem. Eng. J.* **2017**, *311*, 153–162. [[CrossRef](#)]
80. Heckert, E.G.; Karakoti, A.S.; Seal, S.; Self, W.T. The role of cerium redox state in the SOD mimetic activity of nanocerium. *Biomaterials* **2008**, *29*, 2705–2709. [[CrossRef](#)] [[PubMed](#)]
81. Orge, C.A.; Órfão, J.J.; Pereira, M.F.; de Farias, A.M.D.; Fraga, M.A. Ceria and cerium-based mixed oxides as ozonation catalysts. *Chem. Eng. J.* **2012**, *200*, 499–505. [[CrossRef](#)]
82. Ouyang, W.; Zhou, Y.; Fei, X.; Bai, Y.; Wang, H.; Wu, Z. Simultaneous removal of NO and dichloromethane (CH<sub>2</sub>Cl<sub>2</sub>) over Nb-loaded cerium nanotubes catalyst. *J. Environ. Sci.* **2022**, *111*, 175–184. [[CrossRef](#)] [[PubMed](#)]
83. Xu, L.; Wang, J. Magnetic nanoscaled Fe<sub>3</sub>O<sub>4</sub>/CeO<sub>2</sub> composite as an efficient Fenton-like heterogeneous catalyst for degradation of 4-chlorophenol. *Environ. Sci. Technol.* **2012**, *46*, 10145–10153. [[CrossRef](#)]
84. Karunakaran, C.; Gomathisankar, P.; Manikandan, G. Preparation and characterization of antimicrobial Ce-doped ZnO nanoparticles for photocatalytic detoxification of cyanide. *Mater. Chem. Phys.* **2010**, *123*, 585–594. [[CrossRef](#)]
85. Sin, J.-C.; Lam, S.-M.; Lee, K.-T.; Mohamed, A.R. Preparation and photocatalytic properties of visible light-driven samarium-doped ZnO nanorods. *Ceram. Int.* **2013**, *39*, 5833–5843. [[CrossRef](#)]
86. Cymes, B.A.; Almquist, C.B.; Krekeler, M.P. Europium-doped cryptomelane: Multi-pathway synthesis, characterization, and evaluation for the gas phase catalytic oxidation of ethanol. *Appl. Catal. A Gen.* **2020**, *589*, 117310. [[CrossRef](#)]
87. Chong, M.N.; Jin, B.; Chow, C.W.; Saint, C. Recent developments in photocatalytic water treatment technology: A review. *Water Res.* **2010**, *44*, 2997–3027. [[CrossRef](#)] [[PubMed](#)]
88. Kajjumba, G.W.; Marti, E.J. A review of the application of cerium and lanthanum in phosphorus removal during wastewater treatment: Characteristics, mechanism, and recovery. *Chemosphere* **2022**, *309*, 136462. [[CrossRef](#)] [[PubMed](#)]
89. Kajjumba, G.W.; Attene-Ramos, M.; Marti, E.J. Toxicity of lanthanide coagulants assessed using four in vitro bioassays. *Sci. Total Environ.* **2021**, *800*, 149556. [[CrossRef](#)] [[PubMed](#)]
90. Gonzalez, V.; Vignati, D.A.; Leyval, C.; Giamberini, L. Environmental fate and ecotoxicity of lanthanides: Are they a uniform group beyond chemistry? *Environ. Int.* **2014**, *71*, 148–157. [[CrossRef](#)] [[PubMed](#)]
91. Ghadiri, M.; Ghasemi Darehnaei, M.; Sabbaghian, S.; Shirazian, S. Computational simulation for transport of priority organic pollutants through nanoporous membranes. *Chem. Eng. Technol.* **2013**, *36*, 507–512. [[CrossRef](#)]

**Disclaimer/Publisher’s Note:** The statements, opinions and data contained in all publications are solely those of the individual author(s) and contributor(s) and not of MDPI and/or the editor(s). MDPI and/or the editor(s) disclaim responsibility for any injury to people or property resulting from any ideas, methods, instructions or products referred to in the content.